Topological phases, edge modes, and the Hofstadter butterfly in coupled Su-Schrieffer-Heeger systems

Karmela Padavić, Suraj S. Hegde, Wade DeGottardi, and Smitha Vishveshwara

Phys. Rev. B **98**, 024205 — Published 27 July 2018

DOI: 10.1103/PhysRevB.98.024205

Topological phases, edge modes, and the Hofstadter butterfly in coupled Su-Schrieffer-Heeger systems

Karmela Padavić,[1,*] Suraj S. Hegde,[1,†] Wade DeGottardi,[2,‡] and Smitha Vishveshwara[1,§]

[1] *Department of Physics, University of Illinois at Urbana-Champaign, Urbana, Illinois 61801-3080, USA*
[2] *Joint Quantum Institute, College Park, Maryland 20742, USA*

Motivated by recent experimental realizations of topological edge states in Su-Schrieffer-Heeger (SSH) chains, we theoretically study a ladder system whose legs are comprised of two such chains. We show that the ladder hosts a rich phase diagram and related edge mode structure dictated by choice of inter-chain and intra-chain couplings. Namely, we exhibit three distinct physical regimes: a topological hosting localized zero energy edge modes, a topologically trivial phase having no edge mode structure, and a regime reminiscent of a weak topological insulator having unprotected edge modes resembling a "twin-SSH" construction. In the topological phase, the SSH ladder system acts as an analog of the Kitaev chain, which is known to support localized Majorana fermion end modes, with the difference that bound states of the SSH ladder having the same spatial wavefunction profiles correspond to Dirac fermion modes. Further, inhomogeneity in the couplings can have a drastic effect on the topological phase diagram of the ladder system. In particular for quasiperiodic variations of the inter-chain coupling, the phase diagram reproduces Hofstadter's butterfly pattern. We thus identify the SSH ladder system as a potential candidate for experimental observation of such fractal structure.

I. INTRODUCTION

The advent of the Su-Schrieffer-Heeger (SSH) model [1, 2] as a description of organic chains was a milestone in the study of condensed matter systems in that it offered one of the first realizations of fractionalization. It was shown that a simple tight-binding chain having two different alternating bond strengths between lattice sites hosts localized bound states at its ends, enabling fractionalization for charge at these ends. Subsequently, the model has been studied as a prototype for fractionalization and associated topological properties characterized by band-structure based invariants and localized edge modes. Recent cutting edge experimental developments in diverse disciplines have revealed aspects of the SSH model and related systems in fascinating ways. In cold atomic setting, measurements of topological invariants, such as the Zak phase have been performed [3]. Topologically robust charge pumping has been observed [4–6] where the transported charge is quantized and solely determined by the topology of the pump cycle. Equally striking, topological systems carrying dispersionless edge modes have been realized in magneto-optical photonic crystals [7], classical acoustic meta-materials [8, 9] and even tunable mechanical systems of granular particles [10]. Further, the solitonic state distinguishing the topological phase of the SSH model in particular, has been observed in cold atomic systems [11, 12] through time-of-flight imaging and in photonic quantum walks [13].

Here, we show that the simplest of next steps in these studies—coupling two SSH chains [14–19]— gives rise to rich behavior. We investigate salient features of such "SSH ladder systems", theoretically studying several physical properties with an eye towards realizing them in the experimental settings mentioned above. We chart out the phases exhibited by the the SSH ladder and the phase boundaries separating them as characterized by a gap in the energy spectrum. We determine the topological nature of these phases. We identify the nature and behavior of bound states localized at the ends of the ladder which ought to be realizable in cold atomic, photonic and mechanical settings. We focus on three noteworthy aspects of the SSH ladder. i) The most general phase diagram for the SSH ladder hosts phases that go beyond that of a single chain. These phases show the distinction between completely trivial phases characterized by the absence of edge modes, robust topological phases having topologically protected edge modes, and an intermediate coupling regime having unprotected edge modes. ii) The SSH ladder can act as a model of the Kitaev wire by mimicking its traits in the sense of the Kitaev wire hosting Majorana bound states, which are of much current interest. iii) The SSH ladder system has enough degrees of freedom to exhibit marked effects of inhomogeneous couplings; we focus on the case of (quasi)periodicity.

Parallels between the SSH ladder and the Kitaev chain are of particular significance. To elaborate, the Kitaev chain [20] has come to the forefront as a key model for capturing essential features of topological superconductors. A distinctive feature of the model is a clean phase diagram separating trivial phases from topological ones in which the chain harbors end bound states that are the right combination of particle-like and hole-like excitations for forming charge neutral Majorana fermionic states. The phase diagram for the Kitaev chain, the nature of edge modes and their experimental realization have been thoroughly studied and the Majorana edge states themselves are known to have unique proper-

* kpadavi2@illinois.edu
† shegde2@illinois.edu
‡ wdegott@umd.edu
§ smivish@illinois.edu

ties [20–24]. For the Kitaev chain, a basis can be chosen so that the system admits a ladder description [25]. Remarkably, we find that the SSH ladder is capable of mimicking this Kitaev chain ladder when subject to restricted couplings. We demonstrate how these parallels become manifest. A significant distinction is that the bound states of the SSH ladder are not Majorana fermions but number-conserving states, either fermionic or bosonic in nature. Nevertheless, the SSH ladder provides a concrete experimentally realizable system that can map the phase diagram for the Kitaev chain and the spatial structure of its localized bound edge states.

Extensive work on the Kitaev chain has revealed the manner in which inhomogeneities can greatly alter topological phase diagrams, for instance, periodic variations or disorder [25]. Borrowing from these insights, we show that indeed spatially varying coupling in the SSH ladder system can produce dramatically different phase diagrams. We employ a transfer matrix technique to directly target the fate of localized end modes in the presence of such spatial variations. Further, we find that quasiperiodic variations across the ladder reflect the mathematical structure of Harper's equation and its physical manifestation in Hofstadter's butterfly pattern [26] – one of the most well-known examples of fractals in condensed matter physics. While cold atomic systems are well suited for clean achievement of such self-similar patterns (otherwise experimentally rather challenging in electronic systems), experiments concerning the Hofstadter Hamiltonian so far [27–30] have not included any direct measurements of its fractal nature. As the topological phases of the SSH ladder can be identified through direct observation of edge wavefunction spatial profiles, our proposal provides a novel possibility of probing this fractal diagram through time-of-flight imaging.

In what follows, in Sec. II we introduce the SSH ladder Hamiltonian and outline the use of the momentum space dispersion relation, the chiral index topological invariant and the tranfer matrix formalism in obtaining its phase diagram. In Sec. III we briefly review the properties of a single, uncoupled, SSH chain and proceed to discuss the more complex phase diagram of the coupled system in Sec. IV. In this section, we identify three distinct regimes (topological, topologically trivial and weakly topological) as determined by differing edge mode structures. In Sec. V we focus on the phase of the ladder hosting edge modes with wavefunctions having spatial profiles matching those of the localized Majorana modes of the Kitaev chain. Further, in Sec VI we employ transfer matrix methods to discuss the response of this Kitaev chain analog phase to inhomogenous couplings and disorder. Finally, in Sec. VII we bring our discussion closer to experimental studies of SSH models by considering finite size effects and offer an outlook on possible future experimental work in Sec. VIII.

II. MODEL AND METHODS

The system of interest, shown in Fig. (1), is a fermionic ladder composed of two coupled SSH chains. It exhibits a particle-hole symmetry which arises from the bipartite nature of the Hamiltonian. Consequently, its energy spectrum is symmetric about zero energy. As detailed in Sec. V, when the couplings respect certain constraints, the system is a close analog to the celebrated superconducting Kitaev chain; particle-hole symmetry in this case is a natural consequence of superconductivity, as captured by the Bogoliubov-de Gennes form of its Hamiltonian. The close relationship between the two systems gives rise to a clear correspondence between their respective topological phases. As will be shown, however, rather than hosting Majorana fermions, the topological phases of the SSH ladder are characterized by Dirac fermions localized at the system edge. As detailed in Sec. IV, the more generalized ladder system shows a rich phase diagram. We note here that several of single-particle properties studied in what follows apply to bosonic systems as well. Additionally, similar models have been explored in Ref. [14–16].

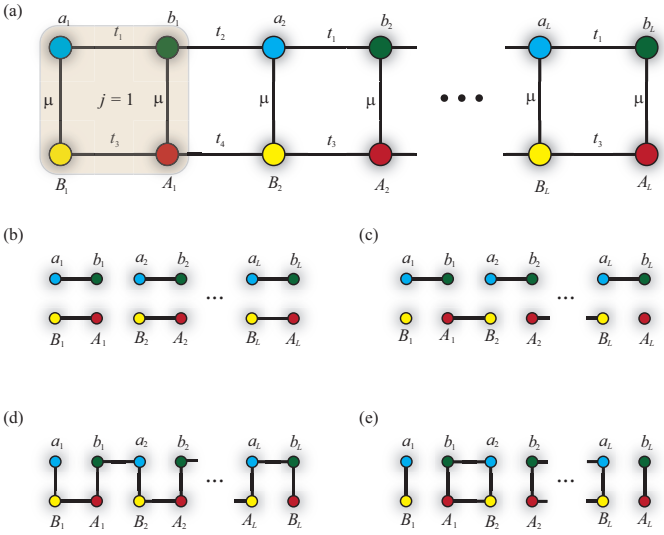

FIG. 1. Pictorial representation of the fermion couplings in the SSH ladder model, as represented by the Hamiltonian (1) for (a) generic couplings, (b) for the decoupled case with the special values of couplings $t_2 = t_3 = 0$ characterized by $N_S = 1$ exhibiting a single fermion end mode, (c) coupled SSH ladder for $t_1 = t_4 = 0$ and $t_2 = t_3 = t$. For $|\mu| < 2|t|$, the system exhibits a Kitaev-like topologically protected zero mode. (e) For $t_1 = t_3 = 0$ and $|\mu| \ll t_2, t_4$, the system exhibits mid-gap states that are not topologically protected.

Model— The unit cell for the SSH ladder is a plaquette composed of four fermions: for the j^{th} plaquette, the operators a_j, b_j are fermion annihilation operators for sites on the top leg, while the operators B_j and A_j

reside on the bottom leg. The Hamiltonian is given by

$$H = \sum_j (t_1 b_j^\dagger a_j + t_2 a_{j+1}^\dagger b_j + t_3 A_j^\dagger B_j + t_4 B_{j+1}^\dagger A_j + \text{h.c.}) + \mu \sum_j (a_j^\dagger B_j + b_j^\dagger A_j + \text{h.c.}). \quad (1)$$

The Hamiltonian H is characterized by five real couplings: four hopping amplitudes t_1, t_2, t_3, and t_4 and an inter-chain coupling μ. The system is bi-partite in that it decouples into two interpenetrating sub-lattices, a/A and b/B coupled to each other but not within themselves. This bi-partite nature of the model guarantees that the spectrum respects particle-hole symmetry. Fourier transforming Eq. (1) yields

$$H_k = \frac{1}{2}\tau_z \otimes [((t_1 - t_3) + (t_2 - t_4)\cos k)\sigma_x + (t_2 + t_4)\sin k\, \sigma_y] + \frac{1}{2}\mathbb{I} \otimes [((t_1 + t_3) + (t_2 + t_4)\cos k)\sigma_x + (t_2 - t_4)\sin k\, \sigma_y] + \mu \tau_x \otimes \sigma_x \quad (2)$$

where the Pauli matrices τ_i and σ_i act in the ladder leg and sublattice spaces, respectively.

Our analyses of the phases and their properties primarily employ three methods. i) For systems respecting translational invariance, energy dispersions obtained in momentum space identify gapless energy contours which delineate phase boundaries. ii) A topological invariant enables us to identify topological aspects of the phases. iii) A transfer matrix technique charts out the existence and nature of possible localized end bound states in some phases. We proceed to elaborate on each of these methods.

Dispersion— First, to establish phase boundaries, we consider the dispersion relation corresponding to Eq. (2). Contours in parameter space along which the bulk energy gap closes delimit different phases of the system. In the most general case, the SSH ladder has a four-band energy dispersion

$$E^2 = \mu^2 + \frac{1}{2}(|\rho_1|^2 + |\rho_2|^2) \pm \frac{1}{2}\sqrt{(2\mu^2 + |\rho_1|^2 + |\rho_2|^2)^2 + 4(\rho_1\rho_2 - \mu^2)(\mu^2 - \rho_1^*\rho_2^*)} \quad (3)$$

where

$$\rho_1 = \rho_1(k) = t_1 + t_2 e^{-ik}$$
$$\rho_2 = \rho_2(k) = t_3 + t_4 e^{+ik}. \quad (4)$$

Here, the gap in the energy spectrum closes at $k = 0$ for $\mu^2 = (t_1 + t_2)(t_3 + t_4)$ while the same happens for $\mu^2 = (t_1 - t_2)(t_3 - t_4)$ and $k = \pi$. Additionally, the energy spectrum is gapless for $t_1 t_4 = t_2 t_3$ and $k = (1/2)\cos^{-1}(\mu^2 - t_1 t_3 - t_2 t_4)/(t_1 t_4 + t_2 t_3))$.

Following Ref. [31], we parameterize the couplings in Eq. (1)

$$t_1 = (t + \Delta)(1 - \eta),\ \ t_2 = (t - \Delta)(1 + \eta),$$
$$t_3 = (t - \Delta)(1 - \eta),\ \ t_4 = (t + \Delta)(1 + \eta). \quad (5)$$

with $|\eta| < 1$, $|\Delta| < t$. In the next section, we offer a physical interpretation for these two parameters in terms of competing energy gaps. Various topological and topologically trivial phases of the ladder are separated by regions in the (μ, Δ, η, t) parameter space satisfying

$$\mu^2 = 4(t^2 - \Delta^2\eta^2),$$
$$\mu^2 = 4(t^2\eta^2 - \Delta^2),\ \text{for}\ t|\eta| > |\Delta|$$
$$\Delta = 0. \quad (6)$$

Topological invariant— Phases of the SSH ladder can be characterized by a topological invariant. The over-arching Hamiltonian of Eq. (1) belongs to the BDI symmetry class and has phases described by a $\mathbb{Z}-$valued topological invariant. Following Refs. [31, 32] we consider the chiral index associated with a generic symmetry operator S with the properties $SH_kS^{-1} = -H_k$, $S^2 = \mathbb{I}$. The topological invariant is given by

$$N_S = \text{Tr}\int_{-\pi}^{\pi} \frac{dk}{4\pi i} S g^{-1}\partial_k g \quad (7)$$

where $g(k) = H^{-1}(k)$ is the Green's function at zero energy.

Transfer matrix— The transfer matrix formalism extensively used in studies of localized states in 1D systems, especially in the presence of potential landscapes, is applicable to this ladder model. We employ this formalism to study the effects of spatial modulation of the inter-chain coupling μ in Sec. VI. This method has been further developed as a tool in studies of Majorana modes in the Kitaev wire by two of the authors in Refs. [22, 25, 33].

Within this formalism, the presence of localized zero energy edge modes is determined by the growth or decay of the eigenfunctions of the transfer matrix. To construct the matrix, we start with the zero-energy Heisenberg equations of motion, $[a_j, H] = 0$, $[b_j, H] = 0$, for

$$H = -\sum_j [t_1(b_{j+1}^\dagger a_j + B_{j+1}^\dagger A_j) + t_2(a_{j+1}^\dagger b_j + A_{j+1}^\dagger B_{2,j})] + \sum_j \mu_j a_j^\dagger B_j + \text{h.c.}$$

where the inter-chain coupling μ_j now varies throughout the ladder. The zero energy equations of motion couple the a_i and A_i fermions and the b_i and B_i fermions, but these two sets of equations have no mutual couplings. The equations of motion for operators a_j are second-order difference equations of the form

$$t(1 + \delta)a_{j-1} + t(1 - \delta)a_{j+1} + \mu_j A_j = 0. \quad (8)$$

Here we have taken $t_1 = t(1 - \delta)$ and $t_2 = t(1 + \delta)$ This can be cast into the form of transfer matrices:

$$\begin{pmatrix} a_{j-1} \\ A_j \end{pmatrix} = A_j \begin{pmatrix} A_j \\ a_{j+1} \end{pmatrix},\ \mathcal{A}_j = \begin{pmatrix} \frac{\mu_n}{t(1+\delta)} & -\left(\frac{1-\delta}{1+\delta}\right) \\ 1 & 0 \end{pmatrix}. \quad (9)$$

Thus, the transfer matrix relates wavefunction amplitudes between one slice of the ladder and its adjacent one.

Its multiplicative nature allows us to study the manner in which the wavefunction varies along the ladder. For localized states, such variation is an exponential decay and can be ascertained based on the eigenvalue structure of the transfer matrix. Such an analysis will be presented in more detail and used extensively in following sections involving inhomogenous variations in the SSH ladder (Sec. VI).

III. SINGLE SSH CHAIN

Before discussing the intricacies of the full model, we briefly recapitulate the properties of a single SSH chain having coupling t_1 and t_2. The chain possesses two topologically distinct phases where the topological and trivial phases are characterized by the presence and absence of end zero modes, respectively. For instance, in the case in which $t_2 = 0$, and $t_1 \neq 0$, the system is described by pairs of coupled fermions. In contrast, for $t_1 = 0$ and $t_2 \neq 0$, the system forms pairs of dimers with the exception of the modes a_1 and b_L which are left uncoupled to the rest of the chain. Particle-hole symmetry guarantees that they are zero energy modes.

The existence of these end bound state fermions is protected by the existence of the bulk energy gap. Tuning away from the special case in which $t_1 = 0$, the end zero mode is a linear combination of modes near the edge of the system. These modes persist as long as the bulk gap does not close. The spectrum of the single SSH chain is given by $E = \pm\sqrt{t_1^2 + t_2^2 + 2t_1 t_2 \cos k}$, and thus the bulk gap closes at $k = \pm\pi$ for $t_1 = t_2$. This condition separates the trivial phase from the topological phases. For $t_1 > t_2 > 0$, the system is trivial. For $t_2 > t_1 > 0$, the system is topological and possesses a single Dirac fermion at each of its ends.

We note that our assignment of phases as topological and topologically trivial depends on where, within the unit cell, we propose a measurement to detect the zero edge state should occur (where a "cut" occurs). In other words, determining the wavefunction spatial profile at a site off-set by half of the unit cell width would result in a different characterization of the phases of the SSH ladder. However, the two previously discussed phases, remain *topologically distinct* regardless. Below, we use a convention consistent with studying the zero mode wavefunctions at the left-most and right-most sites of the SSH ladder.

IV. PHASES OF THE SSH LADDER

As suggested by the phases of the SSH chain, the topology of the ladder system depends sensitively on the relative strengths of the couplings t_1, t_2, t_3, and t_4. As discussed below, we find three distinct physical regimes: a topological phase analogous to the Kitaev chain hosting localized zero energy edge modes, a topologically triv-

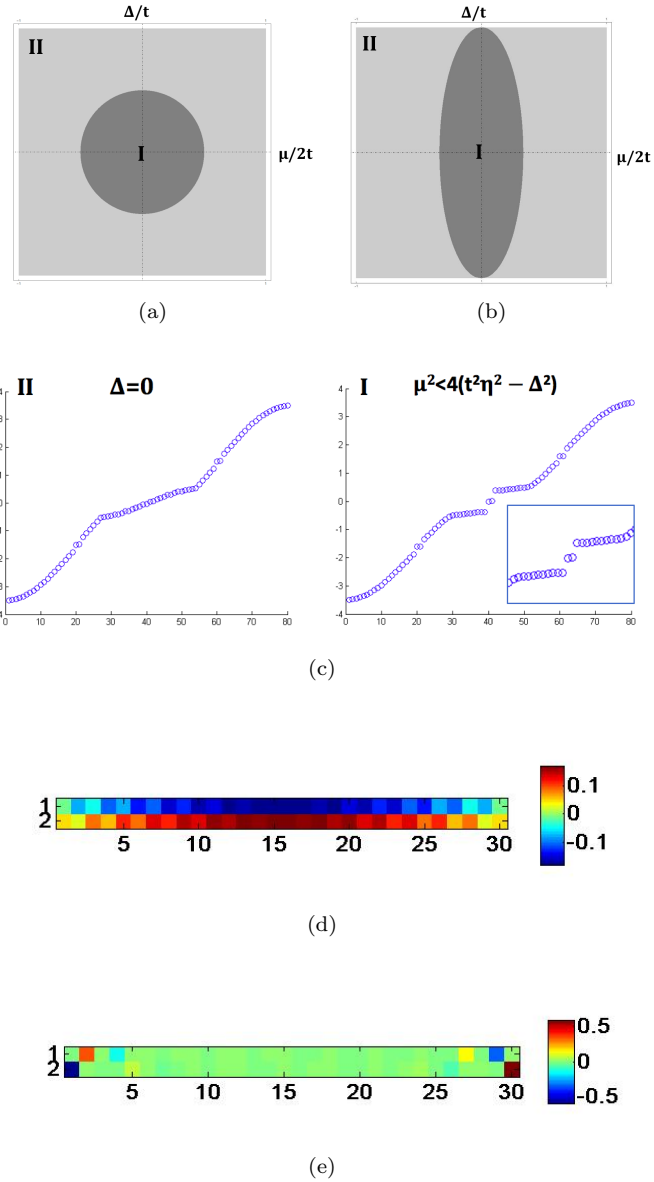

FIG. 2. (a) Phase diagram of the general SSH ladder for $|\Delta| < |\eta|t$. This parameter regime corresponds to a ladder configuration composed of two *identical* SSH chains, as in Fig. 1 (b). Here, phase I hosts a single pair of zero energy edge modes while phase II is topologically trivial having no zero edge mode structure. (b) Phase diagram of the general SSH ladder for $|\Delta| > |\eta|t$. Here, the SSH ladder is in a regime illustrated by Fig. 1 (c) where the two SSH chains that comprise it are *offset* with respect to the relative strength of couplings: if the bottom chain starts with a weaker coupling then the top starts with the stronger one. As in (a), phase I hosts a single pair of zero energy edge modes and phase II supports no zero edge modes. (c), (d) and (e) Energy spectra and spatial wavefunction profiles obtained by numerical diagonalization of the Hamiltonian Eq. (2), corresponding to the phases in (a) and (b). In either parameter regime $\Delta = 0$ describes a gapless line in the phase diagram, having the same dispersion relation as the topologically trivial phase II, as illustrated in (d). The sign of Δ determines whether a_i, A_i or b_i, B_i modes are localized to a particular side of the ladder. (e) shows an example of a topologically nontrivial phase with localized zero energy modes at the edge.

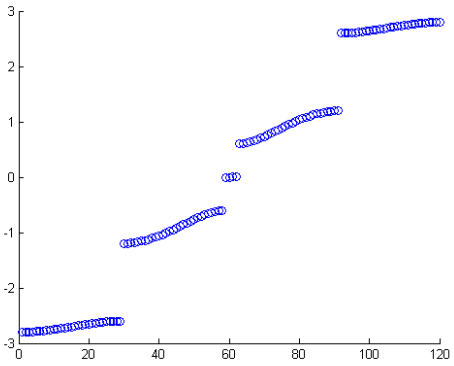

(a)

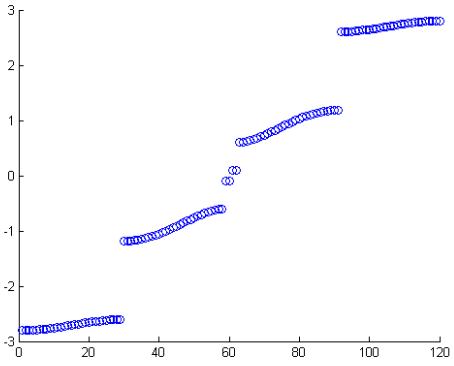

(b)

FIG. 3. Energy spectra obtained by numerical diagonalization of the Hamiltonian Eq. (2), for (a) a fully decoupled SSH ladder $\mu = 0$ and (b) a weakly coupled $\mu \ll 1$ SSH ladder. A non-zero value of the inter-chain coupling μ causes the four zero energy states to hybridize, resulting in non-zero energy mid-gap edge modes.

ial phase and a regime analogous to a weak topological insulator having unprotected edge modes resembling a "twin-SSH" construction. To provide an intuitive picture for these phases, in considering Fig. 1, it is clear that in addition to a topologically trivial phase having no localized edge modes (Fig. 1 (b)) the SSH ladder can host a single localized mode at each edge (Fig. 1 (c)) or two pairs of localized modes at each edge as in Fig. 1 (e).

The parameters Δ and η introduced in Eq. (5) quantify the relative strengths of the various dimerization patterns that the SSH can exhibit. The quantity η is indicative of the relative strength of inter-plaquette and intra-plaquette couplings, while Δ is a measure of how strongly the upper and lower legs of the ladder have opposite dimerization patterns. In particular, increasing Δ, for $t, \Delta > 0$ tends to give rise to a single end mode on each end of the chain. This mode has weight on the a_i, A_i modes on the left-hand side of the chain and the b_i, B_i modes on the right-hand side. Similarly, decreasing Δ for $\Delta < 0$ tends to localize a single fermion with the roles of a_i, A_i and b_i, B_i interchanged. The parameter η treats the upper and lower legs symmetrically. For $\eta > 0$, there is a tendency to localize two fermionic modes to each end of the ladder.

The topological nature of the phases can be characterized by tailoring the topological invariant introduced in Eq. 7 to the SSH ladder. In particular, identifying $S = \mathbb{I} \otimes \sigma_z$, we obtain

$$N_S = -\int_{-\pi}^{\pi} \frac{dk}{2\pi i} \partial_k \log(t_1 t_3 + t_2 t_4 + t_2 t_3 e^{-ik} + t_1 t_4 e^{ik} - \mu^2). \quad (10)$$

The topological index N_S is thus the winding number of an ellipse in the complex plane. If the ellipse does not enclose the origin, the system is trivial and $N_S = 0$. This occurs for

$$\mu^2 > (t_1 + t_2)(t_3 + t_4) = 4(t^2 - \Delta^2 \eta^2). \quad (11)$$

For

$$(t_1 - t_2)(t_3 - t_4) = 4(t^2\eta^2 - \Delta^2) < \mu^2 \quad (12)$$
$$< (t_1 + t_2)(t_3 + t_4) = 4(t^2 - \Delta^2\eta^2), \quad (13)$$

the ellipse encloses the origin and $N_S = \mathrm{sgn}(t\Delta)$. The sign of N_S thus determines whether a_i, A_i or b_i, B_i modes are localized to a particular side of the ladder. The two possible cases are therefore topologically distinct and separated by a gapless line $\Delta = 0$ in the topological phase diagram as in, for instance, Fig. (2).

Given that the ladder is essentially two coupled SSH chains, *a priori* the system seems capable of hosting zero, one or two localized modes at its ends. Our analysis of the topological invariant N_S shows that this expectation is not quite accurate. We find that there are two distinct topological phases which exhibit single fermionic zero modes at each end of the ladder. At the same time, the ladder system cannot host more than one fermionic mode at each end. In particular, the form of N_S in Eq. (10) makes it clear that only if the ladder has longer range hopping can $|N_S| > 1$.

We can also address the fate of the zero modes for two topological SSH chains which are coupled. The two end modes can hybridize, thus forming the analog of a weak topological insulator, as shown in 1 (e). A single fermion mode is however protected given that for a spectrum with particle hole symmetry and an odd number of states there must be at least one zero energy state. This argument is readily generalized: for a system of N chains coupled by weak inter-channel couplings, we anticipate that a topological phase (with a single topological edge mode) will result if and only if the number of chains that are topological is odd, a natural consequence of fermion parity and particle-hole symmetry.

We remark that while the hybridization of edge states in the case of two coupled chains does not allow for a topological phase hosting zero energy edge states, the resulting regime is distinct from the trivial regime in that there is a persistent, non-zero energy, bound state at each

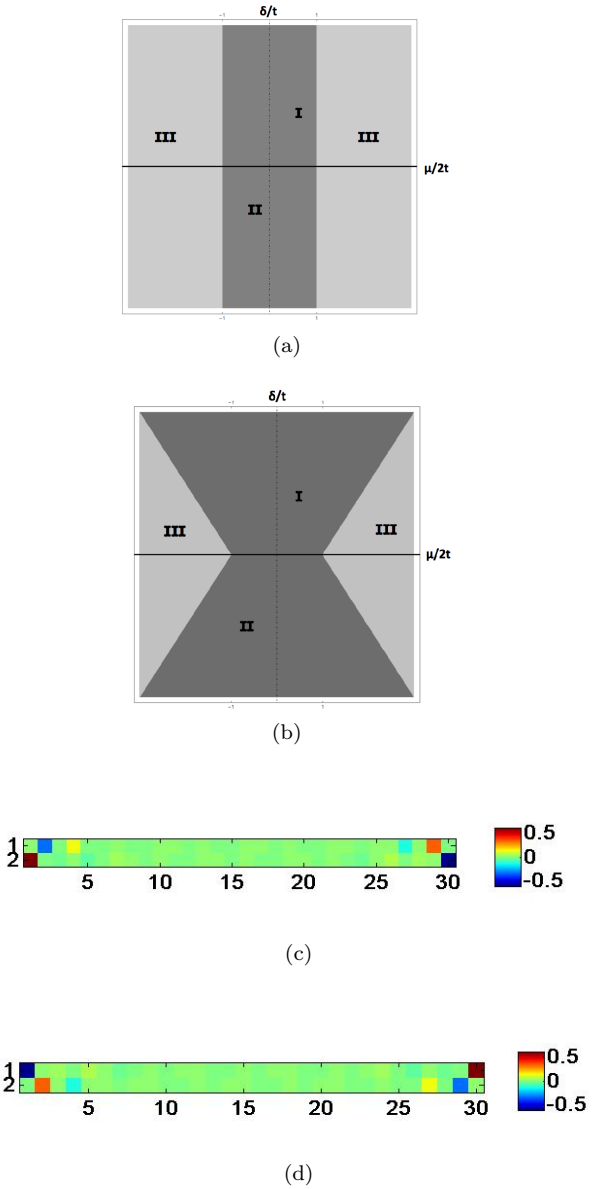

FIG. 4. (a) Phase diagram for an infinitely long SSH ladder with $t_1 = t_3$ and $t_2 = t_4$, (b) phase diagram for an SSH ladder with hopping parameters as in (a) and a finite size L. The slope of the phase boundaries is linear in L. (c) and (d) Spatial wavefunction profiles corresponding to the two topologically non-trivial phases (I and II in (a)) of the reduced SSH ladder.

ladder end. As shown in Fig. 3, hybridization causes the bound edge states to move away from zero energy but they still form low-energy mid-gap states. Transitioning into the trivial state having no boundary modes whatsoever requires the closing of the bulk energy gap.

V. KITAEV CHAIN ANALOG

We now specialize to the case in which $\eta = 0$. We take $t_1 = t_4 = t(1-\delta)$, $t_2 = t_3 = t(1+\delta)$, where $\delta = \Delta/t$. As discussed in the previous section, δ measures the tendency of the SSH ladder to have the opposite dimerization patterns on the upper and lower legs, respectively. Thus, larger $|\delta|$ tends to stabilize topologically non-trivial phases.

This special, restricted set of couplings offers a means of probing the phase diagram of the Kitaev chain, a prototype for studying Majorana wires and the exciting physics of Majorana fermionic bound states [20, 34]. The Kitaev chain consists of a single chain of electrons possessing on-site local chemical potential μ that can tunnel between sites (for instance, with strength t) and experience nearest neighbour p-wave pairing (for instance, of strength Δ). When represented in terms of pairs of Majorana fermions on each site, the physical construction exactly maps on to the SSH ladder with the identification $t_{1/2} = t \pm \Delta$ [25]. Electronic bound states at the ends of the SSH ladder map to Majorana fermionic bound states at the end of the Majorana wire. Most importantly, the dispersions for both systems are identical and the phase boundaries serve to demarcate topological phases from trivial ones.

Specifically, in the Kitaev chain analog limit, the energy dispersion of the SSH ladder takes the form

$$E_{\pm}(k) = \pm t\sqrt{(2\cos(k) + \mu/t)^2 + (2\delta\sin(k))^2}. \quad (14)$$

As in Sec. IV, the loci of energy gap closing points form the phase boundaries between different topological phases of the system and are given by : $\mu = \pm 2t$ at $k = 0, \pi$ and $\delta = 0$ at $k = \cos^{-1}(-\mu/2t)$. The phase diagram determined by these curves is shown in Fig. 4 (a). The topology of the various parts of the phase diagram are readily established by considering simple cases. The $\delta = -1$ corresponds to the case shown in Fig. 1 (d) which can be viewed as a single SSH chain weaving between the upper and lower legs of the ladder. In accordance with findings for a single, disconnected, chain the system is topologically non-trivial in this case provided that $|\mu| < 2|t|$.

To re-emphasize the connections and differences between the SSH ladder and the Kitaev chain, the Dirac fermionic end modes in the SSH ladder correspond to phases with end Majorana modes in the Kitaev chain. Though sometimes attributed to the $\mathbb{Z}_2$ character of the Kitaev chain (a system in class D), we see that this property is actually due to particle-hole symmetry and fermionic parity. Indeed, when the superconducting order parameter is taken to be real in the Kitaev chain, the Hamiltonian is also in the BDI class.

VI. INHOMOGENEOUS COUPLINGS AND THE HOFSTADTER BUTTERFLY

We now consider the effect of including spatial inhomogeneity in a specific coupling terms in the SSH ladder system. In particular, we remain within the Kitaev

chain analog limit of $t_1 = t_4$, $t_2 = t_3$ and consider periodicity, quasi-periodicity, and disorder in the inter-chain coupling μ. Our reason for this is three-fold. First, we wish to preserve particle-hole symmetry and the bipartite nature of the lattice and thus do not include an actual on-site chemical potential. Second, variation in μ for the ladder system exactly maps on to such a variation in a potential landscape in the Kitaev chain, thus enabling us to parallel Majorana fermion physics in the presence of potential landscapes and disorder [25, 35–38]. Third, of the vast parameter space for inhomogeneities, we narrow our study to the most natural choice and show the rich phase diagram structure stemming from even varying a single parameter.

Explicitly, the inter-chain coupling in our model Hamiltonian of Eq. (1) takes the form

$$\sum_{j=1}(\mu_{2j-1}a_j^\dagger B_j + \mu_{2j}b_j^\dagger A_j + \text{h.c.}). \tag{15}$$

The topology of the disordered chain is most conveniently found by employing the transfer matrix method, discussed in Sec. II. We define the Lyapunov exponent of the transfer matrix is $\gamma(\{\mu_j\}, \delta, L) = \lim_{L\to\infty} 1/L \ln|\lambda|$, where λ is its highest eigenvalue. The exponent is the inverse of the localization length of the edge-mode wavefunction in the topological phase. The phase boundaries separating the topologically trivial and non-trivial phases are thus determined by $\gamma = 0$, corresponding to a diverging localization length at the transition point.

To probe the fate of the topological phase diagram when inhomogeneities are present, we make use of a similarity transformation as given in Ref. [22]. Explicitly, the similarity transformation on the full chain transfer matrix is given by

$$\mathcal{A}(\mu_n, \delta) = \left(\frac{1-\delta}{1+\delta}\right)^{N/2} S\tilde{\mathcal{A}}(\mu_n/\sqrt{1-\delta^2}, \delta = 0)S^{-1} \tag{16}$$

where $S = \text{diag}(\ell_\delta^{1/4}, 1/\ell_\delta^{1/4})$ and $\ell_\delta = \frac{1-\delta}{1+\delta}$ and we have set $t = 1$. The matrix $\tilde{\mathcal{A}}_n$ is the transfer matrix for a normal tight-binding model – in the context of quasiperiodicity, a Harper model – in the absence of a dimerization δ. The model's on-site chemical potential terms are re-scaled by the transformation $\mu_n \to \mu_n/\sqrt{1-\delta^2}$. This map allows the Lyapunov exponent to be written as a sum of two components, $\gamma(\mu, \delta) = \gamma_\delta + \gamma_0$, one that depends purely on the dimerization γ_δ and $\gamma_0(\mu/\sqrt{1-\delta^2})$, which is the Lyapunov exponent for a system having no dimerization and a rescaled locally varying chemical potential. Thus, knowing wavefunction properties for non-dimerized system enables identifying localized wavefunctions in an SSH ladder having the same spatial variation.

One-dimensional fermionic systems are especially sensitive to non-uniform potentials and disorder. The similarity transformation quantifies the fact that the tendency to localize fermions directly competes with the topological phases. The transfer matrix formalism is particularly well-suited to the study of spatially varying potentials. The topological phases can be determined by considering the eigenvalues of $\prod_i \mathcal{A}_i$, where the product runs over a full unit cell of the system in question.

More precisely, if both eigenvalues of $\mathcal{A}$ have a magnitude less than 1, this indicates that the a_i/A_i zero mode decays as it goes into the bulk from the right. Since the transfer matrix governing the b_i/B_i mode is given by $\mathcal{A}^{-1}$, in this case the b_i/B_i mode would be localized to the right-hand side of the system. If however $\mathcal{A}$ has one eigenvalue that is larger than 1 in magnitude and

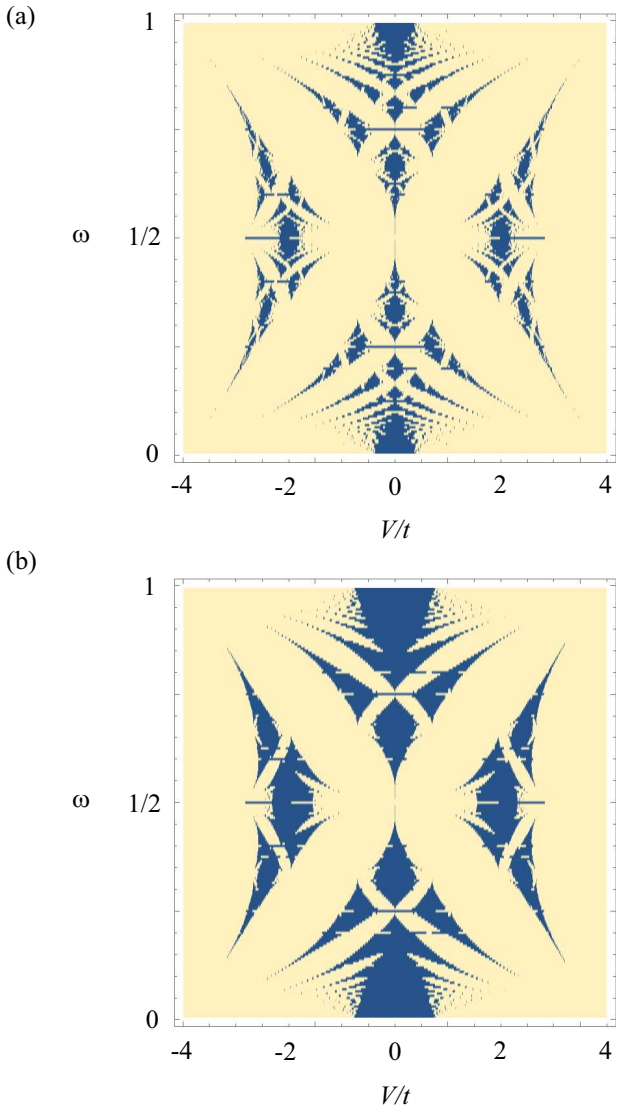

FIG. 5. The phase diagram for a quasiperiodically varying inter-chain coupling $\mu_n/t = V/t + 2\cos(2\pi\omega n)$, where $2t = t_1 + t_2$, reflects the Hofstadter butterfly pattern. The lighter regions indicate the places where the bulk gap closes and the Lyapunov exponent vanishes i.e. the topologically trivial regions. The Hofstadter butterfly pattern shows loci in parameter space where available energy states exist in the limit $\delta = t_1 - t_2 = 0$. These loci seed topological phases, which occupy larger regions of the phase diagram as δ grows larger between panels (a) $\delta = 0.1$ and (b) $\delta = 0.2$.

another that is smaller than 1, then the zero modes are not normalizable and thus this case corresponds to the trivial phase.

Physically, the topology of the Kitaev-like ladder is dictated by the competition between the coupling parameters μ/t and $\delta = \Delta/t$. The parameter δ breaks the symmetry between the a_1 and B_1 modes at the left end of the chain. In the limit $\delta = 0$, the Hamiltonian treats the a_i/A_i and b_i/B_i modes symmetrically, and thus must be trivial since the topologically non-trivial modes are characterized by a *single* end mode. For $0 < \delta \leq 1$, the coupling of the a_1 mode to the rest of the chain is weakened relative to the B_1 mode, and thus in this case any topological phase will have $N_S = 1$.

We begin our investigation of inhomogenously coupled SSH chains with a particulary simple case which illustrates the relevant physics. Consider the case in which $\delta = -1$ (recall that we have set $t = 1$) and μ_n is some arbitrary configuration (either periodic, quasiperiodic, or disordered). As discussed above, this case can be considered as a single connected chain as in Fig. 1 (d). In this case, the product of transfer matrices can be carried out explicity

$$\prod_{n=1}^{N} \mathcal{A}_n = \frac{1}{(2t)^N} \prod_{n=1}^{N} \mu_i \begin{pmatrix} 1 & 0 \\ 2t/\mu_1 & 0 \end{pmatrix}. \tag{17}$$

The eigenvalues of the resultant matrix are $\frac{1}{(2t)^N} \prod_{n=1}^{N} \mu_n$ and zero. The phase is topological provided that the nonzero eigenvalue has magnitude less than 1. The condition that the system is topological can be expressed as

$$\langle \ln (|\mu_n|/t) \rangle \leq \ln 2, \tag{18}$$

a condition that is applicable to periodic, quasiperiodic, and disordered potentials. We point out that this special case ($\delta = -1$) can be mapped to the disordered quantum Ising model. In this correspondence, the topological phase in the fermionic system corresponds to the ferromagnetic phase in the spin model.

In discussing modulations of the inter-chain coupling μ_n, of particular note is the case in which

$$\mu_n/t = V/t + 2\cos(2\pi\omega n). \tag{19}$$

This variation is of particular interest in the context of localization physics and arises in the problem of an electron on a two-dimensional lattice in a magnetic field. The spectrum of the latter is fractal and is known as Hofstadter's butterfly. The fractal pattern arises due to ω continuously tuning through quasi-periodic and periodic modulations with respect to the underlying lattice. In the present notation, Hofstadter's butterfly corresponds to the regions in which the Lyapunov exponent for Eq. (19) and δ are zero. Given the similarity transformation discussed above, knowing Lyapunov exponents in the Hofstadter case enables us to derive Lyapunov exponents for non-zero δ. This in turn enables us to determine the regions of parameter space that support localized end bound states and are thus topological.

We have plotted the topological phase diagram in the $V-\omega$ plane for two values of δ in Fig. 5. As δ is increased from zero, the mapping to Hofstadter's model indicates that the regions corresponding to the lowest Lyapunov exponent get filled in first. Thus, as δ is increased from zero, regions of the phase diagram nearest to available energy states reflected in the Hofstadter butterfly pattern become topological first. As noted above, increasing δ tends to isolate an a_i/A_i mode, giving rise to more regions which are topological. The phase diagram shown in Fig. 5 ultimately arises as a result of the competition between the localizing potential μ_n given by Eq. (19) and the effects of nonzero δ.

Our treatment above of spatial variations in the inter-chain coupling μ is generic and allows for different forms of variation. Disorder in μ is another natural choice. The extensive treatments of such a case for the Kitaev chain [22] immediately translate to the phase diagrams expected for the SSH ladder system.

VII. FINITE SIZE

In experimental set-ups, for instance cold-atomic optical lattices, the number of lattice sites in the system is typically quite small due to limitations of experimental techniques. Consequently, finite size effects are a significant consideration in experimental observation of topological phases. We thus derive the structure of edge mode wavefunctions for a system of size 'L' and demonstrate how a phase boundary can be effectively obtained through finite-size analyses.

For the reduced SSH ladder model – the analogue of the Kitaev wire discussed in Sec. V – it is sufficient to consider the Fourier space Hamiltonian

$$\hat{H}_k^1 = \begin{pmatrix} 0 & \rho(k) \\ \rho^*(k) & 0 \end{pmatrix} \tag{20}$$

where $\rho(k) = t_1 e^{ika} + t_2 e^{-ika} + \mu$ and $\rho(k) = |\rho(k)| e^{i\phi(k)}$. This Hamiltonian, Eq. (20), connects to the larger Hamiltonian of Eq. (2) through a unitary transformation U that renders the latter off-diagonal and defines A and B sub-lattices that are linear combinations of a and A (b and B):

$$U^\dagger \hat{H}_k U = \begin{pmatrix} \hat{H}_k^1 & 0 \\ 0 & \hat{H}_k^1 - 2\mu\sigma_x \end{pmatrix} \tag{21}$$

and $(A_k^\dagger, B_k^\dagger) = \frac{1}{\sqrt{2}}(a_k^\dagger + A_k^\dagger, b_k^\dagger + B_k^\dagger)$.

The eigenstates of Eq. (20), corresponding to two eigenvalues $\pm E$, are of the form:

$$|u_k, \pm\rangle = \frac{1}{\sqrt{2}} \begin{pmatrix} e^{-i\phi(k)} \\ \pm 1 \end{pmatrix}. \tag{22}$$

Here, the phase $\phi(k)$ is implicitly given by

$$\cot\phi(k) = \frac{t_1 + t_2}{t_1 - t_2} \cot k + \frac{\mu}{t_1 - t_2} \csc k. \tag{23}$$

We construct the edge mode states as linear combinations $|v_k,\pm\rangle = C_+|u_k,\pm\rangle + C_-|u_{-k},\pm\rangle$. Further, in terms of lattice wavefunctions [39]:

$$|u_k,\pm\rangle = \sqrt{\frac{1}{2L}}\sum_{j=1}^{L}\begin{pmatrix} e^{-i\phi(k)} \\ \pm 1 \end{pmatrix} \times(e^{ikj}|j,A\rangle, e^{ik(j+1)}|j+1,B\rangle) \quad (24)$$

where A and B denote the same sublattices as above.

To analyze the effects of the ladder's finite size we impose open boundary conditions and require that the wave functions vanish for sites $j = 0, L+1$. More precisely, we set

$$\langle 0,B|v_k,\pm\rangle = 0 \\ \langle (L+1),A|v_k,\pm\rangle = 0. \quad (25)$$

Enforcing these conditions leads us to identify phase boundaries as a function of δ, t, μ and the system size L as

$$\frac{t_1 - t_2}{t_1 + t_2 - \mu} = \frac{\delta}{2t-\mu} = L+1. \quad (26)$$

As shown in Fig. 4 (b), for the Kitaev wire analogue SSH ladder having finitely many lattice sites, the slope of phase boundaries is linear in system size. For large system sizes ($L \to \infty$), the boundaries become vertical and match the phase boundaries in the thermodynamic limit. Further, enforcing Eq. (25) enables us to obtain the form of the wavefunctions of zero energy edge modes:

$$|v_{k_\lambda},\pm\rangle = \frac{1}{\sqrt{L}}\sum_{j=1}^{L}\begin{pmatrix} \sinh(\lambda_\xi a(L+1+j)) \\ \pm\sinh(\lambda_\xi(j+1)a) \end{pmatrix} \times(|j,A\rangle, |j+1,B\rangle) \quad (27)$$

where λ_ξ is the inverse of the localization length ξ for the edge state. In other words, λ_ξ is equivalent to the Lyapunov exponent γ of Sec. V.

When $L >> \xi$ i.e. the system size is much larger than the localization length, the difference in energy of the modes corresponding to the two states in Eq. (27) decreases exponentially fast with increasing L so that for a large yet finitely-sized system the edge modes are effectively degenerate states with vanishing energies. The 'bending' of the phase boundaries compared to the phase diagram of Fig. 4 (a) for a ladder with a finite size and the qualitative shape of the edge-mode wavefunction in Eq. (27) are germane to experimental studies of the SSH ladder system.

Further, we use the same formalism to compare the general SSH ladder to its decoupled $\mu \to 0$ limit. Considering the case in which the decoupled system consists of two topological chains i.e. two chains hosting a pair of zero egde modes, these four modes can be described by the wavefunctions

$$|v^{\rm ab}_{k_\lambda},\pm;v^{\rm AB}_{k_\lambda},\pm\rangle = \sum_{j=1}^{L}\frac{(-1)^{j+1}}{\sqrt{L}}\begin{pmatrix} \sinh(\lambda_\xi(L+1-j)) \\ \pm\sinh(j\lambda_\xi) \\ \sinh(j\lambda_\xi) \\ \pm\sinh(\lambda_\xi(L-j+1)) \end{pmatrix} \times(|j,a\rangle, |j,b\rangle, |j,A\rangle, |j,B\rangle) \quad (28)$$

with λ_ξ as above. An addition of a small inter-chain coupling μ can then be treated perturbatively. Consequently, we see that regardless of the size of the SSH ladder, the four zero energy edge states acquire an energy shift linear in μ. In other words, these modes hybridize and the energy spectrum does not possess any zero modes but rather two pairs of non-zero energy midgap states, as shown in Fig. (3). This observation is consistent with our previous discussion of pairs of zero edge modes not being topologically protected, as in Sec. IV.

VIII. OUTLOOK

In summary, we have analyzed the SSH ladder as a natural extension of the well-studied SSH chain, paying particular regard to topological and edge state properties. We have charted the phase diagram exhibited by such a ladder system and pinpointed the nature of the topological phases. Under a restricted set of couplings, the ladder serves as an analog for the Kitaev chain and associated Majorana physics. In this regime, we have investigated the effect of inhomogeneity and the possibility of a 'topological Hofstadter butterfly phase diagram' for quasiperiodic variations. With an eye towards realizing these features in a variety of experimental systems, we have discussed the role played by finite size effects.

One particularly elegant realization of localized edge modes in the context of cold atomic experiments has already been achieved in Ref. [11], where these topological features of a single SSH chain have been confirmed through direct imaging. The procedure of directly detecting edge-localization entails loading condensate atoms on a particular lattice 'site', which in this experimental setup corresponds to a discrete momentum state, and suddenly turning on, or quenching, the desired coupling between sites. Observing consequent population decay, or the lack thereof, to the neighboring 'sites' through time-of-flight absorption imaging then indicates whether or not a zero energy edge mode is supported for this point in the space of couplings. Such images comprise a direct observation of an edge mode and confirm that the system is in a topologically nontrivial phase. An extension of such methods to our SSH ladder would required a setup capable of realizing two coupled chains and the ability to tune through parameter space in order to access our predicted phase diagrams.

A similar procedure for observing edge modes has been used in a photonic system [13], where a photon is initialized next to the boundary between two topologically distinct quantum walks and observed to not spread ballisti-

cally when a bound edge state is present. In metamaterials of Ref. [9], the zero modes are found to localize in the corners of the system and to be robust to mechanical deformations corresponding to changes in the space of inter- and intra-chain couplings. These systems thus offer various means of manifesting Kitaev chain analogs through SSH ladder realizations. The Majorana fermion bound states in these cases would translate to Dirac fermionic, bosonic, and even classical mechanical localized modes confined to ends of the ladder.

Turning to inhomogeneity, the appearance of the Hofstadter butterfly is one of many exotic features arising from the rich mathematical structure of the Harper equation and related quasi-periodicity. Quantities of interest such as the wavefunctions and the density of states are known to have multifractality [40]. Recently there have been works on realising a quasiperiodic system through a Hofstadter Hamiltonian in cold atomic systems [27, 28]. Even though cold atomic systems are well suited for realizations of complex structures such as the Hofstadter butterfly in contrast to electronic systems, recent experimental studies centered on the Hofstadter Hamiltonian have not included any direct measurements of the fractal character of the system's wavefunctions. Our model of coupled SSH chains provides a novel possibility of realizing this striking self-similar diagram through observation of topological phases driven by direct time-of-flight imaging and related experimental techniques described above.

ACKNOWLEDGMENTS

We are grateful to Diptiman Sen, Bryce Gadway, Alex An, Eric Meier and Taylor Hughes for useful discussions. This work is supported by the National Science Foundation under the grant DMR 0644022-CAR.

[1] W. P. Su, J. R. Schrieffer, and A. J. Heeger, Phys. Rev. Lett. **42**, 1698 (1979).
[2] A. J. Heeger, S. Kivelson, J. R. Schrieffer, and W. P. Su, Rev. Mod. Phys. **60**, 781 (1988).
[3] M. Atala, M. Aidelsburger, J. T. Barreiro, D. Abanin, T. Kitagawa, E. Demler, and I. Bloch, Nature Physics **9**, 795 (2013).
[4] M. Lohse, C. Schweizer, O. Zilberberg, M. Aidelsburger, and I. Bloch, Nature Physics **12**, 350 (2016).
[5] S. Nakajima, T. Tomita, S. Taie, T. Ichinose, H. Ozawa, L. Wang, M. Troyer, and Y. Takahashi, Nature Physics **12**, 296 (2016).
[6] L. Wang, M. Troyer, and X. Dai, Phys. Rev. Lett. **111**, 026802 (2013).
[7] Z. Wang, Y. Chong, J. D. Joannopoulos, and M. Soljacic, Nature **461**, 772 EP (2009).
[8] R. Süsstrunk and S. D. Huber, Science **349**, 47 (2015), http://science.sciencemag.org/content/349/6243/47.full.pdf.
[9] W. C. Peterson, W. A. Benalcazar, T. L. Hughes, and G. Bahl, ArXiv e-prints (2017), arXiv:1710.03231 [cond-mat.mes-hall].
[10] R. Chaunsali, E. Kim, A. Thakkar, P. G. Kevrekidis, and J. Yang, Phys. Rev. Lett. **119**, 024301 (2017).
[11] E. J. Meier, F. A. An, and B. Gadway, Nature Communications **7**, 13986 (2016).
[12] M. Leder, C. Grossert, L. Sitta, M. Genske, A. Rosch, and M. Weitz, Nature Communications **7**, 13112 (2016).
[13] T. Kitagawa, M. A. Broome, A. Fedrizzi, M. S. Rudner, E. Berg, I. Kassal, A. Aspuru-Guzik, E. Demler, and A. G. White, Nature Communications **3**, 882 (2012).
[14] L. Li, Z. Xu, and S. Chen, Phys. Rev. B **89**, 085111 (2014).
[15] S.-L. Zhang and Q. Zhou, Phys. Rev. A **95**, 061601 (2017).
[16] J.-Y. Zou and B.-G. Liu, ArXiv e-prints (2015), arXiv:1506.06626 [cond-mat.str-el].
[17] J.-W. Rhim, J. H. Bardarson, and R.-J. Slager, ArXiv e-prints (2017), arXiv:1710.01466 [cond-mat.str-el].
[18] D. Bercioux, O. Dutta, and E. Rico, ArXiv e-prints (2016), arXiv:1609.06292 [cond-mat.mes-hall].
[19] J. I. Vayrynen and T. Ojanen, Phys. Rev. Lett. **107**, 166804 (2011).
[20] A. Kitaev, Phys. Usp. **44**, 131 (2001).
[21] J. Alicea, Reports on Progress in Physics **75**, 076501 (2012).
[22] W. DeGottardi, M. Thakurathi, S. Vishveshwara, and D. Sen, Phys. Rev. B **88**, 165111 (2013).
[23] S. R. Elliott and M. Franz, Rev. Mod. Phys. **87**, 137 (2015).
[24] M. Leijnse and K. Flensberg, Semiconductor Science and Technology **27**, 124003 (2012).
[25] W. DeGottardi, D. Sen, and S. Vishveshwara, Phys. Rev. Lett. **110**, 146404.
[26] D. R. Hofstadter, Phys. Rev. B **14**, 2239 (1976).
[27] M. Aidelsburger, M. Atala, M. Lohse, J. T. Barreiro, B. Paredes, and I. Bloch, Phys. Rev. Lett. **111**, 185301 (2013).
[28] H. Miyake, G. A. Siviloglou, C. J. Kennedy, W. C. Burton, and W. Ketterle, Phys. Rev. Lett. **111**, 185302 (2013).
[29] K. Osterloh, M. Baig, L. Santos, P. Zoller, and M. Lewenstein, Phys. Rev. Lett. **95**, 010403 (2005).
[30] D. Jaksch and P. Zoller, New Journal of Physics **5**, 56 (2003).
[31] R. Wakatsuki, M. Ezawa, Y. Tanaka, and N. Nagaosa, Phys. Rev. B **90**, 014505 (2014).
[32] V. Gurarie, Phys. Rev. B **83**, 085426 (2011).
[33] W. DeGottardi, D. Sen, and S. Vishveshwara, New J. Phys. **13**, 065028 (2011).
[34] S. S. Hegde and S. Vishveshwara, Phys. Rev. B **94**, 115166 (2016).
[35] J. Sau and E. Demler, Phys. Rev. B **88**, 205402 (2013).
[36] M.-T. Rieder, P. W. Brouwer, and I. Adagideli, Phys. Rev. B **88**, 060509 (2013).
[37] M.-T. Rieder and P. W. Brouwer, Phys. Rev. B **90**, 205404 (2014).
[38] P. Neven, D. Bagrets, and A. Altland, New Journal of Physics **15**, 055019 (2013).

[39] P. Delplace, D. Ullmo, and G. Montambaux, Phys. Rev. B **84**, 195452 (2011).

[40] H. HIRAMOTO and M. KOHMOTO, International Journal of Modern Physics B **06**, 281 (1992).